Cortical Flow-Driven Shapes of Nonadherent Cells

A. C. Callan-Jones,[1,*] V. Ruprecht,[2] S. Wieser,[3] C. P. Heisenberg,[2] and R. Voituriez[4,5]
[1]Laboratoire Matière et Systèmes Complexes, CNRS/Université Paris-Diderot, UMR 7057, 75205 Paris Cedex 13, France
[2]Institute of Science and Technology Austria, 3400 Klosterneuburg, Austria
[3]Division of Biomedical Physics, Innsbruck Medical University, 6020 Innsbruck, Austria
[4]Laboratoire Jean Perrin, UMR 8237 CNRS/UPMC, 4 Place Jussieu, 75005 Paris, France
[5]Laboratoire de Physique Théorique de la Matière Condensée, CNRS UMR 7600, Université Pierre et Marie Curie, 75005 Paris, France
(Received 6 July 2015; published 15 January 2016)

Nonadherent polarized cells have been observed to have a pearlike, elongated shape. Using a minimal model that describes the cell cortex as a thin layer of contractile active gel, we show that the anisotropy of active stresses, controlled by cortical viscosity and filament ordering, can account for this morphology. The predicted shapes can be determined from the flow pattern only; they prove to be independent of the mechanism at the origin of the cortical flow, and are only weakly sensitive to the cytoplasmic rheology. In the case of actin flows resulting from a contractile instability, we propose a phase diagram of three-dimensional cell shapes that encompasses nonpolarized spherical, elongated, as well as oblate shapes, all of which have been observed in experiment.

DOI: 10.1103/PhysRevLett.116.028102

Cell shapes are highly varied, ranging from spheroidal [1–4], to spread out and flattened [5], to dendritic [6]. They are dynamic and can undergo large changes, having functional roles in cell polarization, migration, division, and the early stages of embryonic development.

While the role of biochemical pathways in regulating cell shapes has been recognized, for example, in cell division [7], the shape of a cell is ultimately determined by the balance of forces acting in the cellular medium. The mechanical properties of eukaryotic cells are, to a great extent, governed by the cytoskeleton and in particular the actin-myosin system, a dynamic meshwork of semi-flexible polymers. The actin cytoskeleton is not only responsible for passive rheological properties of cells, but also generates, by ATP hydrolysis, active stresses in the cell [8–11].

A striking consequence of these active stresses are cytoskeletal flows at the cell scale. These flows can now also be induced in biomimetic systems [12]. Cortical flows are vital to cell migration [1–4,13–16]; recently, they have been shown to contribute to the regulation of cell polarity [17–21] and to the formation of the contractile ring in cell division [22]. In the well-studied case of adherent cells on planar substrates, the impact of actin flows on cell shape has been analyzed [5], and the flattened, bean shape of keratocytes has been captured by several models [23–26]. In this context, a theoretical analysis of possible cell shapes of nonadherent cells is missing, and general rules to determine these shapes have yet to be proposed.

In this Letter, we focus on recent observations of shapes of nonadherent cells of various types, which emerge concomitantly with large-scale, polarized actin flows in the cell cortex [1,2]. Modeling the cortex as a layer of active gel, we show that cortical tension anisotropy, induced by cortical flows, can account for the observed pear-shaped, elongated phenotype. We demonstrate that the predicted shapes are related directly to the cortical flow, and are independent of the underlying mechanism generating the flow. We propose a phase diagram of cell shapes—largely independent of the cytoplasmic rheology—that accounts for observations of (nonpolarized) spherical, elongated [1,2], as well as oblate, shapes [3].

Model and general considerations.—Before considering the instability mechanism giving rise to cortical flow, we first show that simple relations link it to cell shape. Motivated by experiments on breast tumor cells [3] and on zebrafish progenitor cells [1], we consider a polarized cell, assumed axisymmetric about the z axis, with a cortical velocity field given by $\mathbf{v} = v\hat{\boldsymbol{\theta}}$ along its surface in spherical coordinates; see Fig. 1(c). Note that we are taking a perturbative approach to find the cell shape: for a steady state $v(\theta)$, expressed on the undeformed, spherical cell, we find the resulting cell deformation. This approach assumes that v is small—that the cell is not far from the instability threshold—and that the mechanical compliance of the cell is also small (to be made more precise below). This compliance depends on the cytoplasmic rheology, which is complex and not well characterized *in vivo*. Yet, it is commonly described as fluid at long times, due, partly, to cytoskeletal filament turnover. At short times, elastic behavior has been reported, mainly due to long-lived structures such intermediate filaments and organelles [27]. Below, we model the cytoplasm as a viscous fluid; in [28], we treat it as an elastic medium. This approach, which covers both limits of viscoelastic models is, thus, general, and with it, we find that the cell shape does not depend strongly on cytoplasmic rheology.

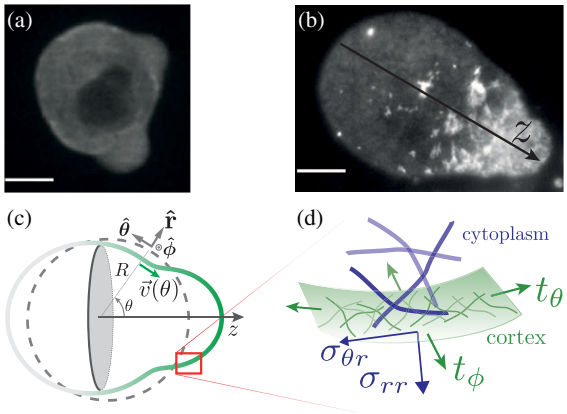

FIG. 1. Cell polarization and shape change. (a) Unpolarized zebrafish cell. (b) Elevated contractility leads to polarization. Cortical flows in the direction of $z > 0$, with a corresponding gradient in cortical actomyosin density (myosin II labeled with green fluorescent protein). (c) Deformed cortical surface (calculated as described below) is shown in green, and unpolarized reference state is given by gray dashed line. To lowest order, flow is parallel to $\hat{\boldsymbol{\theta}}$. (d) A cortical patch, with tensions t_θ and t_ϕ, in contact with cytoplasm, with stress $\underline{\underline{\sigma}}$. Images in (a) and (b) are from Ref. [1]. Scale bars in (a) and (b) are 10 μm.

We now write down the cortical tension components in the polarized state, as shown in Fig. 1(d). To this end, we model, separately, the actomyosin dynamics giving rise to cortical tension and the resulting mechanical response of the cell. We treat the cortex as a compressible active fluid with density ρ. Similar to Refs. [1,32], we do not consider the cortical thickness changes that might result from instability. We write the total cortical tensions as $t_\theta = T_0 + T_\theta$ and $t_\phi = T_0 + T_\phi$ where T_0 is the tension (cortex plus membrane) in the initial, nonpolarized state, and T_θ and T_ϕ are the tension changes in the cortex upon polarization. We then write T_θ and T_ϕ in a generic form, separating anisotropic, flow-dependent terms from an isotropic, v-independent one, $T_{\rm i}(\rho)$ [a particular form will be given in Eq. (11)]

$$T_\theta = \frac{2\eta}{R}\partial_\theta v + T_Q + T_{\rm i}, \tag{1a}$$

$$T_\phi = \frac{2\eta}{R}\cot\theta v - T_Q + T_{\rm i}. \tag{1b}$$

In the above, the flow-dependent tension components consist of viscous parts, with (two-dimensional) cortical viscosity η, and terms $\pm T_Q$ that depend on the orientational order of cortical filaments. We have neglected the contribution of the radial velocity of the cortex to the strain rates along the unit vectors $\hat{\boldsymbol{\theta}}$ and $\hat{\boldsymbol{\phi}}$, consistent with our perturbative approach. In general, velocity gradients in a fluid composed of anisotropic constituents couple to nematic order [33,34]. Following Ref. [34], we introduce the in-plane (traceless) nematic order parameter whose principal components are $Q_{\theta\theta} = \tilde{Q}$ and $Q_{\phi\phi} = -\tilde{Q}$. Note that $\tilde{Q} > 0$ (<0) implies filament alignment parallel to $\hat{\boldsymbol{\theta}}$ ($\hat{\boldsymbol{\phi}}$). Ordering of active filaments leads to anisotropic, active tensions $T_Q = \zeta'\tilde{Q}$ along $\hat{\boldsymbol{\theta}}$ and $-T_Q$ along $\hat{\boldsymbol{\phi}}$, where $\zeta' > 0$ [34]. In the absence of flow, the cortex is assumed to be deep in the isotropic phase, and therefore, $\tilde{Q}$ adiabatically follows gradients of v: $\tilde{Q} = (\beta_1/\chi R)(\partial_\theta - \cot\theta)v$, where $\beta_1 > 0$ is the flow alignment parameter and $\chi > 0$ is the inverse nematic susceptibility. Therefore,

$$T_Q \simeq \frac{\zeta'\beta_1}{\chi R}(\partial_\theta - \cot\theta)v. \tag{2}$$

At mechanical equilibrium, and neglecting inertia, a cortical element satisfies the force balance

$$\frac{1}{R}\partial_\theta T_\theta + \frac{\cot\theta}{R}(T_\theta - T_\phi) = \sigma_{\theta r}|_R, \tag{3}$$

where $\sigma_{\theta r}|_R$ is the shear stress in the cytoplasm at the cell surface, $r = R$.

We now present the three results of this Letter.

Shape is controlled by cortical flow.—In particular, for a given $v(\theta)$, the shape does not depend on the specific instability model giving rise to flow, as contained in the choice of $T_{\rm i}(\rho)$. This result is obtained as follows.

The shape is determined through Laplace's law, which to linear order in the surface displacement $u(\theta)\hat{\mathbf{r}}$, is

$$\sigma_{rr}|_R = -2T_0\delta H - \frac{T_\theta + T_\phi}{R}, \tag{4}$$

where $2\delta H = -(R^2\sin\theta)^{-1}\partial_\theta(\sin\theta\partial_\theta u) - 2R^{-2}u$ is the change at $\mathcal{O}(u)$ in the total curvature, relative to $2H_0 = 2/R$. Using Eq. (4), we can directly relate u to v.

To find u, we calculate the cortical tensions, $\Sigma T \equiv T_\theta + T_\phi$ and $\Delta T \equiv T_\phi - T_\theta$, and the cytoplasmic stresses at the surface in terms of v. To do so, the surface variables are projected onto Legendre polynomials: $f(\theta) = \sum_l f_l P_l(\cos\theta)$, $g(\theta) = \sum_l g_l P_l^1(\cos\theta)$, and $h(\theta) = \sum_l h_l P_l^2(\cos\theta)$, where $f = u$, $2\delta H$, ΣT, or $\sigma_{rr}|_R$; $g = v$ or $\sigma_{\theta r}|_R$; and $h = \Delta T$. Notably,

$$2\delta H_l = \frac{1}{R^2}(l-1)(l+2)u_l, \tag{5}$$

and, thus, generally nonzero for $l > 1$.

Next, ΣT, appearing in Laplace's law, can be related solely to v, circumventing its dependence on ρ. Using Eqs. (1)–(2) and recurrence properties of Legendre polynomials [35], we find

$$\Delta T_l = -\frac{2\tilde{\eta}}{R}v_l, \tag{6}$$

where $\tilde{\eta} = \eta + \zeta'\beta_1/\chi$; thus, we see that, as relates to cell shape, filament alignment renormalizes the cortical viscosity, and is, therefore, not needed, per se, to explain the observed shapes. Using this intermediate result and Eq. (3), we obtain

$$\Sigma T_l = \frac{2\tilde{\eta}}{R}(l-1)(l+2)v_l + 2R(\sigma_{\theta r}|_R)_l. \tag{7}$$

To find the surface stresses, assuming fluid cytoplasmic behavior, we note that since cytoplasmic flow near the cortex is of order v, $\sigma_{rr}|_R \sim \sigma_{\theta r}|_R \sim \mu v/R$, where μ is the cytoplasm viscosity. In comparison, the viscous contributions of T_θ and T_ϕ to Eqs. (3) and (4) scale as $\eta v/R^2$. Thus, the influence of cytoplasm on cell shape is negligible for $R \lesssim \eta/\mu$. A conservative estimate of η/μ is 1 mm [22], and thus, this inequality holds for most animal cells. A calculation assuming Stokes flow in the cytoplasm allows, nonetheless, the determination of the surface stresses [28]. With these results and with Eqs. (4)–(7), we finally obtain the displacement

$$u_l = -\frac{R}{T_0}\left[\frac{\mu}{l+2} + \frac{2\tilde{\eta}}{R}\right] v_l, \tag{8}$$

for $l > 1$; the $l = 1$ mode is absent since it corresponds to a rigid translation along z. Remarkably, we find that the cell shape can be determined solely from the flow amplitudes, v_l. This result confirms the above scaling argument; thus, we set $\mu = 0$ for the remainder. Scaling then yields $u/R \sim \tilde{\eta} v/T_0$, and thus, our perturbative scheme assumes that $\tilde{\eta} v/T_0 < 1$. Similar expressions to Eq. (8) hold for the projections of the two components of the displacement $\mathbf{u}|_R$ in the case of elastic cytoplasm, as shown in [28]. Thus, direct relations between cortical flow and cell shape hold for quite general cytoplasmic rheology.

Tension anisotropy leads to pearlike shape.—To demonstrate our second result, we truncate the mode expansion at $l = 3$, which is justified if the cortical instability leading to polarization occurs not far above the $l = 1$ instability threshold.

Since polarized zebrafish cells, for instance, are elongated and asymmetric, we expect that a combination of $l = 2$ (symmetric about $\theta = \pi/2$) and $l = 3$ (antisymmetric) can qualitatively account for the observed shape. To proceed further, we calculate the aspect ratio, defined as $\mathcal{A} \equiv [2R + u(0) + u(\pi)]/[2R + 2u(\pi/2)]$. We also calculate the difference between the meridional curvatures at the poles, given by $\Delta\kappa_\theta = 2[\delta H(0) - \delta H(\pi)]$. With Eq. (8), we obtain

$$\mathcal{A} \simeq \frac{R - 2\tilde{\eta} v_2/T_0}{R + \tilde{\eta} v_2/T_0}; \tag{9}$$

a similar expression holds for elastic cytoplasm [28]. Thus, the sign of v_2 determines whether the cell is elongated or flattened by the cortical flow. We also find

$$\Delta\kappa_\theta \simeq -40\frac{\tilde{\eta}}{R^2 T_0} v_3, \tag{10}$$

and thus, the sign of v_3 determines which of the cell, front ($\theta = \pi$) or back ($\theta = 0$), is the more pointed.

Deferring until later the question of what controls the sign of v_2 and v_3, they can be related to the tension anisotropy, ΔT. According to Eq. (6), a negative value of v_2 implies $\Delta T_2 > 0$; since $P_2^2(\cos\theta) = 3\sin^2\theta \geq 0$, $v_2 < 0$ means that, near threshold for instability, we expect $T_\phi \geq T_\theta$. Therefore, negative v_2, leading to $\mathcal{A} > 1$, is consistent with the cell being squeezed perpendicular to, and elongated along, the z axis. In addition, since $P_3^2(\cos\theta) = 15\sin^2\theta\cos\theta$, negative v_3 implies greater cell squeezing perpendicular to the z axis near the cell rear rather than near the front, leading to pear-shaped cells with a pointed rear. Thus, the lowest cortical flow modes can account for the observed shape, and, in particular, cell elongation is a direct consequence of the tension anisotropy stemming from the flow.

Phase diagram of cell shapes.—Finally, we derive a shape phase diagram, as a function of parameters governing cortical actin dynamics. We start by specifying a model for T_i, along the lines of Refs. [1,20,32,36], that drives the cortical instability. T_i contains two terms: one, a molecular motor-generated contractile part that, for sufficient activity, causes instability; and, second, a stabilizing term that smooths the interface between the sparse cell front and the dense cell rear [1]. These effects are captured by

$$T_\mathrm{i} = \zeta\rho + \frac{\gamma}{R^2\sin\theta}\partial_\theta(\sin\theta\partial_\theta\rho), \tag{11}$$

where $\zeta > 0$ is the contractility strength and $\gamma > 0$. In our model, T_i does not depend independently on the density of bound myosin in the cortex, m_b, which is justified by experiments showing that $m_\mathrm{b} \propto \rho$ [1]. We note that our model is closely related to one that considers the cortex as an incompressible active gel in which the thickness is the dynamical variable [22,37]; in that context, the first term above is identified as the constant active stress integrated over the thickness, while the second term arises from interfacial tension between cortex and cytoplasm.

The existence of cortical instability can be seen by linearizing Eqs. (1), (3), (11), and the continuity equation

$$\partial_t\rho + \frac{1}{R\sin\theta}\partial_\theta(\sin\theta\rho v) = -k_\mathrm{d}(\rho - \rho_0), \tag{12}$$

about the nonpolarized state, $v = 0$ and $\rho = \rho_0$. In Eq. (12), we have neglected, as done earlier, the contribution of $\dot{u}/R$ to the strain rates. In this equation, the source term $-k_\mathrm{d}(\rho - \rho_0)$ accounts for actin turnover, at rate k_d. Performing the linearization and assuming $\delta\rho = \rho - \rho_0 = \rho_l e^{\lambda_l t} P_l(\cos\theta)$ and $v = v_l e^{\lambda_l t} P_l^1(\cos\theta)$, we obtain

$$v_l = \frac{R\alpha_l}{\eta}\left(\zeta - \frac{\gamma l(l+1)}{R^2}\right)\rho_l, \tag{13}$$

and the dispersion relation $\lambda_l = -k_d + l(l+1)C_l\rho_0$, where $C_l = \eta^{-1}\alpha_l[\zeta - \gamma l(l+1)/R^2]$ and $\alpha_l = [l(l+1) + (\tilde{\eta}/\eta)(l-1)(l+2)]^{-1}$. The cortical mode l becomes unstable if ζ exceeds $[\gamma l(l+1)/R^2] + (k_d\eta/\rho_0\alpha_l)$. We note that this instability is saturated by the interfacial term in T_i that enters, via cortical force balance [Eq. (3)], the nonlinear, convective term in Eq. (12).

Motivated by experiments on cells [1,3] and on reconstituted systems [12] that reveal a monotonically increasing cortical density and cortical flow directed from front to back, we assume that only the $l = 1$ mode is unstable. By identifying $\theta = 0$ with the cell rear, we are taking ρ_1 and v_1 as positive; since $P_1^1 = -\sin\theta$, $v_1 > 0$ implies flow from front to back, as found experimentally. Thus, we assume $\lambda_1 > 0$, the remaining λ_l s are negative, and $|\lambda_1| \ll |\lambda_2| \ll |\lambda_3|$, etc. At long times after the onset of instability, the cortex reaches a steady, flowing state. It is the nonlinear coupling between the $l = 1$ and higher modes that saturates the instability and that is responsible for the final cell shape.

The types of polarized cell shapes are summarized in Fig. 2, in which k_d and ζ are varied. Above the line $\lambda_1 = 0$ (green) all modes are stable, polarization does not occur, and cells remain spherical; see inset (i). Below this line, the $l = 1$ mode is unstable and elongated, or oblate shapes arise. For small ζ, cells are elongated, as illustrated in inset (ii), and closely resemble polarized zebrafish cells, including the actomyosin-dense, pointed cell rear. For higher ζ, the shape is oblate, as shown in inset (iii), also with a pointed, dense rear.

The shape boundaries in Fig. 2 can be understood by going beyond the linear regime presented above, and performing a weakly nonlinear analysis (WNLA). This is valid for $\lambda_1 \gtrsim 0$, that is, just below the green line in Fig. 2, and we retain couplings between the $l = 1, 2$, and 3 modes. Using Eqs. (12) and (13), and carrying out the integrals of products of three Legendre polynomials in Mathematica [38], we obtain dynamical equations for the density modes, ρ_2 and ρ_3

$$\dot{\rho}_2 = \lambda_2\rho_2 + 2C_1\rho_1^2 + \mathcal{O}(\rho_2^2, \rho_1\rho_3), \tag{14a}$$

$$\dot{\rho}_3 = \lambda_3\rho_3 + \frac{12}{5}(C_1 + 2C_2)\rho_1\rho_2 + \mathcal{O}(\rho_2\rho_3), \tag{14b}$$

where the overdot indicates a time derivative. In the WNLA, $\dot{\rho}_2 \simeq 0$, which, according to Eq. (14a), yields $\rho_2 \simeq 2C_1\rho_1^2/|\lambda_2|$ and, thus, positive according to our hypotheses. As a result, v_2 goes from positive to negative at $\zeta = 6\gamma/R^2$ [see Eq. (13)]. Figure 2 shows that, near $\lambda_1 = 0$, both v_2 and $\mathcal{A} - 1$ change sign at this value of ζ, validating Eq. (9) and confirming the importance of the sign of v_2; farther below the green line, higher modes contribute and the $v_2 = 0$ and $\mathcal{A} = 1$ curves separate. We have numerically solved Eqs. (3) and (12) at steady state, using Eqs. (1)–(2), (4)–(8), and (11), to obtain v_2 and $\mathcal{A}$ [38].

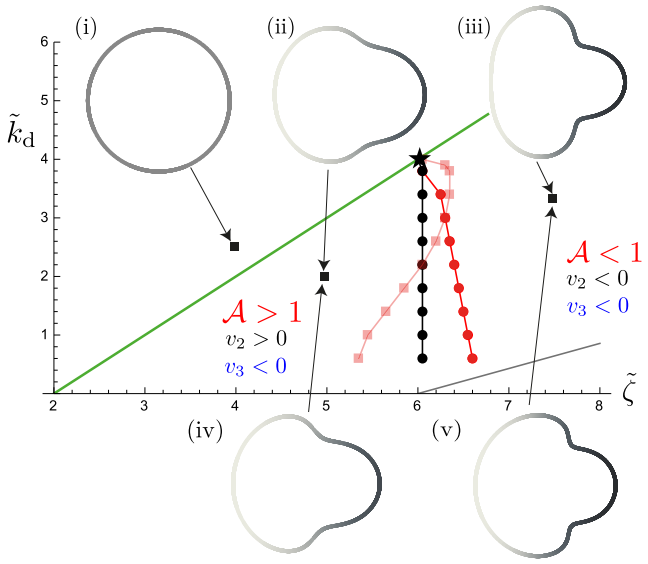

FIG. 2. Shape diagram in (k_d, ζ) plane. The dark (light) red line separates regions of elongated and oblate shapes for a viscous (elastic) cytoplasm. On the black line, $v_2 = 0$. Filled star indicates, for $\lambda_1 \to 0^+$, the point where v_2 vanishes, as obtained by a WNLA. Straight gray line: $\lambda_2 = 0$. Nondimensionalizations: $\tilde{k}_d = k_d\eta R^2/(\gamma\rho_0)$ and $\tilde{\zeta} = \zeta R^2/\gamma$. Cuts along the cell symmetry plane reveal typical shapes for a fluid cytoplasm: (i), $\tilde{\zeta} = 4$, $\tilde{k}_d = 2.5$, $T_0R^2/(\gamma\rho_0) = 20$; (ii), $\tilde{\zeta} = 5$, $\tilde{k}_d = 2$, $T_0R^2/(\gamma\rho_0) = 10.66$; (iii), $\tilde{\zeta} = 7.5$, $\tilde{k}_d = 3.25$, $T_0R^2/(\gamma\rho_0) = 17.33$. Two typical shapes, for an elastic cytoplasm with Young's modulus E and Poisson ratio ν, are shown: (iv), $\tilde{\zeta} = 5$, $\tilde{k}_d = 2$, $ER^3/(\gamma\rho_0) = 8$; (v), $\tilde{\zeta} = 7.5$, $\tilde{k}_d = 3.25$, $ER^3/(\gamma\rho_0) = 22$. Note that, for ease of visualization, we have shown shapes with significant deformations, though the calculations were done using the perturbative approach described in the text. Gray scale along contours indicates ρ/ρ_0 at steady-state: high density is dark, and low is light. ρ is found by solving Eqs. (1)–(3) along with Eqs. (11) and (12). Cortical thickness is not shown to scale. Other parameter values in this figure are $\eta/(\xi R^2) = 25$, $\mu R/\eta = 0$, $\zeta'\beta_1/(\chi\eta) = 1$, and $\nu = 0.5$.

In addition, according to Eq. (14b), $\dot{\rho}_3 \simeq 0$ implies $\rho_3 \simeq \frac{24}{5}|\lambda_2|^{-1}|\lambda_3|^{-1}C_1(C_1 + 2C_2)\rho_1^3$. A short calculation shows, therefore, that $v_3 < 0$ for $12\gamma R^{-2} > \zeta > \gamma R^{-2}(\alpha_1 + 6\alpha_2)(\alpha_1 + 2\alpha_2)^{-1}$. In this range, according to Eq. (10), the cell rear is more pointed than the front, and is confirmed by Fig. 2.

Finally, we point out that the results presented in Fig. 2 do not qualitatively depend on our assumption of a fluid cytoplasm. Assuming elastic behavior [28], we find that the overall cell shape is unchanged [insets (iv) and (v)], and that the boundary separating $\mathcal{A} > 1$ and $\mathcal{A} < 1$ changes only slightly (light red curve). In the case of an elastic cytoplasm, just beneath the cortex, the cytoplasm experiences a shear stress ξv, where ξ is a friction coefficient; consequently, the $l = 1$ mode is relevant to the cell shape

since both radial and tangential displacements, u_r and u_θ, occur.

We have shown, in this Letter, that anisotropic cortical tensions, induced by cortical instability, can be responsible for the typical morphologies of nonadherent cells. We have demonstrated that the characteristic deformations caused by cortical surface flows—elongation versus flattening, and front or back asymmetry—are not very sensitive to the nature of the cytoplasmic mechanical response. Thus, a similar approach could be applied at the tissue scale, where bulk elastic behavior persists on longer time scales. Our model is likely relevant to understanding the shape symmetry-breaking in early developing *Drosophila* embryos by surface cell migration [39] and to deformation occurring during the epiboly stage of zebrafish embryogenesis [40].

V. R. acknowledges support by the Austrian Science Fund (FWF): (Grant No. T560-B17).

*Corresponding author.
andrew.callan-jones@univ-paris-diderot.fr

[1] V. Ruprecht, S. Wieser, A. Callan-Jones, M. Smutny, H. Morita, K. Sako, V. Barone, M. Ritsch-Marte, M. Sixt, R. Voituriez, and C.-P. Heisenberg, Cell **160**, 673 (2015).
[2] Y.-J. Liu, M. Le Berre, F. Lautenschlaeger, P. Maiuri, A. Callan-Jones, M. Heuzé, T. Takaki, R. Voituriez, and M. Piel, Cell **160**, 659 (2015).
[3] R. Poincloux, O. Collin, F. Lizárraga, M. Romao, M. Debray, M. Piel, and P. Chavrier, Proc. Natl. Acad. Sci. U.S.A. **108**, 1943 (2011).
[4] R. J. Hawkins, M. Piel, G. Faure-Andre, A. M. Lennon-Dumenil, J. F. Joanny, J. Prost, and R. Voituriez, Phys. Rev. Lett. **102**, 058103 (2009).
[5] K. Keren, Z. Pincus, G. M. Allen, E. L. Barnhart, G. Marriott, A. Mogilner, and J. A. Theriot, Nature (London) **453**, 475 (2008).
[6] B. Alberts, A. Johnson, J. Lewis, M. Raff, K. Roberts, and P. Walter, *Molecular Biology of the Cell*, 4th ed. (Garland, New York, 2002).
[7] M. Loose, K. Kruse, and P. Schwille, Annu. Rev. Biophys. **40**, 315 (2011).
[8] K. Kruse, J.-F. Joanny, F. Jülicher, J. Prost, and K. Sekimoto, Phys. Rev. Lett. **92**, 078101 (2004).
[9] F. Jülicher, K. Kruse, J. Prost, and J.-F. Joanny, Phys. Rep. **449**, 3 (2007).
[10] M. C. Marchetti, J. F. Joanny, S. Ramaswamy, T. B. Liverpool, J. Prost, M. Rao, and R. A. Simha, Rev. Mod. Phys. **85**, 1143 (2013).
[11] J. Prost, F. Julicher, and J.-F. Joanny, Nat. Phys. **11**, 111 (2015).
[12] E. Abu Shah and K. Keren, eLife **3**, e01433 (2014).
[13] J. A. Theriot and T. J. Mitchison, Nature (London) **352**, 126 (1991).
[14] K. Kruse, J. F. Joanny, F. Jülicher, and J. Prost, Phys. Biol. **3**, 130 (2006).
[15] M. Bergert, A. Erzberger, R. A. Desai, I. M. Aspalter, A. C. Oates, G. Charras, G. Salbreux, and E. K. Paluch, Nat. Cell Biol. **17**, 524 (2015).
[16] A. C. Callan-Jones and R. Voituriez, New J. Phys. **15**, 025022 (2013).
[17] M. Mayer, M. Depken, J. S. Bois, F. Jülicher, and S. W. Grill, Nature (London) **467**, 617 (2010).
[18] N. W. Goehring, P. K. Trong, J. S. Bois, D. Chowdhury, E. M. Nicola, A. A. Hyman, and S. W. Grill, Science **334**, 1137 (2011).
[19] P. Maiuri, J.-F. Rupprecht, S. Wieser, V. Ruprecht, O. Bénichou, N. Carpi, M. Coppey, S. De Beco, N. Gov, C.-P. Heisenberg, C. Lage Crespo, F. Lautenschlaeger, M. Le Berre, A.-M. Lennon-Dumenil, M. Raab, H.-R. Thiam, M. Piel, M. Sixt, and R. Voituriez, Cell **161**, 374 (2015).
[20] J. S. Bois, F. Jülicher, and S. W. Grill, Phys. Rev. Lett. **106**, 028103 (2011).
[21] P. Bun, J. Liu, H. Turlier, Z. Liu, K. Uriot, J.-F. Joanny, and M. Coppey-Moisan, Biophys. J. **107**, 324 (2014).
[22] H. Turlier, B. Audoly, J. Prost, and J.-F. Joanny, Biophys. J. **106**, 114 (2014).
[23] K. Doubrovinski and K. Kruse, Phys. Rev. Lett. **107**, 258103 (2011).
[24] C. Blanch-Mercader and J. Casademunt, Phys. Rev. Lett. **110**, 078102 (2013).
[25] E. Tjhung, D. Marenduzzo, and M. E. Cates, Proc. Natl. Acad. Sci. U.S.A. **109**, 12381 (2012).
[26] E. Tjhung, A. Tiribocchi, D. Marenduzzo, and M. E. Cates, Nat. Commun. **6**, 5420 (2015).
[27] M. Guo, A. J. Ehrlicher, M. H. Jensen, M. Renz, J. R. Moore, R. D. Goldman, J. Lippincott-Schwartz, F. C. Mackintosh, and D. A. Weitz, Cell **158**, 822 (2014).
[28] See Supplemental Material at http://link.aps.org/supplemental/10.1103/PhysRevLett.116.028102 for details of the calculation of the cell deformation, which includes Refs. [29–31].
[29] H. Lamb, *Hydrodynamics*, 6th ed. (Dover Publications, New York, 1945).
[30] A. I. Lur'e, *Three-Dimensional Problems of the Theory of Elasticity* (Wiley Interscience, New York, 1964).
[31] L. D. Landau and I. L. Lifshitz, *Theory of Elasticity* (Butterworth Heinemann, London, 1986).
[32] E. Hannezo, B. Dong, P. Recho, J.-F. Joanny, and S. Hayashi, Proc. Natl. Acad. Sci. U.S.A. **112**, 8620 (2015).
[33] P.-G. de Gennes and J. Prost, *The Physics of Liquid Crystals*, 2nd ed. (Oxford University Press, Oxford, 1993).
[34] G. Salbreux, J. Prost, and J. F. Joanny, Phys. Rev. Lett. **103**, 058102 (2009).
[35] M. Abramowitz and I. Stegun, *Handbook of Mathematical Functions* (Dover Publications, New York, 1965).
[36] R. J. Hawkins, R. Poincloux, O. Bénichou, M. Piel, P. Chavrier, and R. Voituriez, Biophys. J. **101**, 1041 (2011).
[37] G. Salbreux, J. F. Joanny, J. Prost, and P. Pullarkat, Phys. Biol. **4**, 268 (2007).
[38] Mathematica 10.0, Wolfram Research, Inc., Champaign, Illinois, 2014.
[39] D. Bilder and S. L. Haigo, Dev. Cell **22**, 12 (2012).
[40] R. O. Karlstrom and D. A. Kane, Development **123**, 461 (1996).